

Optimizing Event Selection with the Random Grid Search

P. C. Bhat ^{a*}, H. B. Prosper ^{b†}, S. Sekmen ^{c‡}, C. Stewart ^{d§}

^a *Fermi National Accelerator Laboratory,
Batavia, Illinois, 60510-5011, USA*

^b *Department of Physics,
Florida State University,
Tallahassee, Florida 32306, USA*

^c *Kyungpook National University,
Daegu, South Korea*

^d *Broad Institute, Boston, USA*

(Dated: May 14, 2018)

Abstract

The random grid search (RGS) is a simple, but efficient, stochastic algorithm to find optimal cuts that was developed in the context of the search for the top quark at Fermilab in the mid-1990s. The algorithm, and associated code, have been enhanced recently with the introduction of two new cut types, one of which has been successfully used in searches for supersymmetry at the Large Hadron Collider. The RGS optimization algorithm is described along with the recent developments, which are illustrated with two examples from particle physics. One explores the optimization of the selection of vector boson fusion events in the four-lepton decay mode of the Higgs boson and the other optimizes SUSY searches using boosted objects and the razor variables.

arXiv:1706.09907v2 [hep-ph] 10 May 2018

* pushpa@fnal.gov

† harry@hep.fsu.edu

‡ ssekmen@cern.ch

§ stewart@broadinstitute.org

Contents

I. Introduction	2
II. The Random Grid Search	3
A. Algorithm	4
B. Cut types	6
III. Physics examples	6
A. Exploring $H \rightarrow ZZ \rightarrow 4\ell$ with RGS	7
B. Optimizing SUSY razor boost with RGS	12
IV. Summary	16
Acknowledgements	18
A. Using RGS	18
1. Variables and cut directions file	20
2. The RGS class	21
3. Running RGS	23
References	24

I. INTRODUCTION

One of the primary tasks in data analysis is to isolate a potential signal from the background, that is, from the noise, by applying thresholds to one or more discriminating variables. In particle physics, thresholds on discriminating variables are usually referred to as cuts, therefore, for ease of exposition we shall use this terminology throughout this paper.

In many fields, enormous resources are needed to acquire the rapidly growing datasets. It is therefore not surprising that scientists and engineers have devoted considerable effort to develop highly effective methods to extract signals from data. In this paper, we describe a simple and efficient method for finding optimal cuts, called the *random grid search* (RGS), and recent generalizations of it.

Many powerful methods exist to discriminate between different classes of objects that combine multiple variables into a single discriminating function; for example, boosted decision trees and neural networks [1, 2]. These methods have been used with great success in several high-profile particle physics analyses (see, for example, Refs. [3–6]). Such methods are also used routinely in particle identification (see, for example, Ref. [7–10]). Recently, particle physicists have begun to explore the potential of deep neural networks [11–17]. Several tools that implement these methods are readily available for use in high energy physics applications, such as TMVA [18], NeuroBayes [19], Scikit-learn [20], Keras [21], TensorFlow [22, 23] and Theano [24].

However, even when more sophisticated methods are used, it is often useful to select a signal-enhanced dataset by applying optimal cuts to one or more discriminating variables, which could themselves be the outputs of sophisticated multivariate discriminants. It is also demonstrably easier to discern the reason why a particular data sample was selected if the decision is based on the application of cuts, especially if the cuts are to variables with

clear physical meaning. Decision trees gained favor in particle physics precisely because the decisions they furnish are manifest in the cuts they provide. Note, however, that while this is true for a single decision tree, it is not so for the boosted variety, which is an average over many trees. Perhaps the most compelling reason to consider methods based on cuts is that many analyses in particle physics are still cut-based. Therefore, simple efficient methods for finding optimal cuts, such as the random grid search, are still of considerable interest.

The principle behind the random grid search is simple: search for cuts where they are most likely to be useful. Since the goal is to find signal-enhanced regions, it seems reasonable that a cut-based search algorithm focus on signal-like regions rather than explore the entire phase space. Given a large ensemble of sets of cuts, the RGS algorithm applies each set of cuts to a collection of signal and background events and counts the number of signal and background events, s and b , respectively, that pass the cuts. Using these counts, any measure of the quality of the cuts that can be calculated from them, typically a measure of the signal significance, can be used to find the optimal cuts. The key to the effectiveness of the algorithm is the use of importance sampling: the location of the cuts is determined by the distribution of the signal.

The implementation of the RGS algorithm in the software package described in this paper runs sequentially. But, the algorithm can be trivially parallelized, for example by using the CERN package `PROOF` [25]. One could, for example, apply a large number of cuts to multiple signal and background files in parallel.

The random grid search was developed in the early 1990s by Bhat, Prosper and Stewart [26, 27] during the successful search for the top quark at Fermilab [28, 29]. Subsequently, the method was used in several analyses by the D0 Collaboration, including the search for first generation scalar and vector leptoquarks [30] and the measurement of the $t\bar{t}$ cross section [31]. The random grid search algorithm (though not the specific program described here) has been used by the CMS Collaboration in its search for $B_s^0 \rightarrow \mu^+\mu^-$ and $B^0 \rightarrow \mu^+\mu^-$ [32]. It was also used as a central element in [33], which devised a Bayesian method to optimize new physics searches over generic physics models with free parameters. Recently, the algorithm was significantly extended at CERN in the context of various searches for supersymmetry at the LHC using the razor kinematic variables [34]. Clearly, cut-based analyses are still important, which is the motivation for describing here the generalized version of the publicly available RGS package.

The paper is organized as follows. The random grid search algorithm is described in Section II. The utility of the algorithm is illustrated in Section III using a series of examples. The paper is summarized in Section IV. For completeness, the Appendix contains a detailed user manual for the RGS package.

II. THE RANDOM GRID SEARCH

Suppose we wish to select a signal-enriched sample from a large dataset by cutting on two variables x and y . The obvious way is to consider a grid of N^d points $(x_i, y_i), i = 1, \dots, N$, with $d = 2$, quantify the quality of each *cut-point* $(x > x_i)$ and $(y > y_i)$ in separating signal from background, and select the best cut-point. Geometrically, a cut-point is the vertex defined by the lines aligned with the coordinate axes that meet at a point, here (x_i, y_i) , while algebraically it is defined by expressions of the form $(x > x_i) \ \& \ (y > y_i)$. The well-known problem with this approach is the “curse of dimensionality”, the exponentially fast rise in the number of cut-points as N and d increase. The curse is actually much worse

than the numbers imply because the vast majority of cut-points are likely to be highly sub-optimal and therefore useless. Consequently, even if the resources were available to scan billions of cut-points, most of these resources would be wasted.

As alluded to, the key idea of the random grid search (RGS) is to use the *signal distribution* as the distribution of cut-points, a choice that focuses the search for good cuts to the region where they are more likely to be found. By using the signal distribution, resources are focused most efficiently on cuts that best characterize the signal of interest. Note, however, that nothing in RGS precludes the use of distributions other than the signal in order to define the cut-points. For example, in the cases where signals are not exactly known, generic signal distributions can be used for characterizing the signal classes. Since the distribution of the signal determines the cut-points, the lines drawn through them, as illustrated in Figure 1, form a random grid, hence the name of the algorithm. Figure 1 shows the difference between cuts on a regular grid in two dimensions (2-d) and a random grid and illustrates the potential efficiency gain in isolating signal-enriched regions using the RGS algorithm.

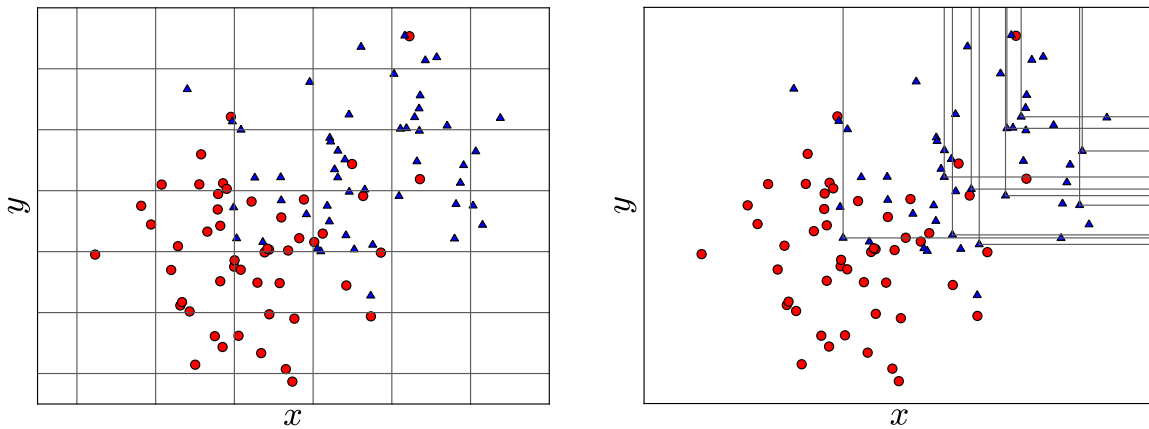


FIG. 1: A regular grid search (left) versus a random grid search (right) in a 2-dimensional space defined by the discriminating variables x and y . The triangles represent the signal events, the circles represent the background events and the lines show the values of x and y where the cuts are applied [27]. Geometrically, a cut-point is the intersection of the lines.

The RGS algorithm is an effective way to optimize a signal's presence over backgrounds in order to discover or measure that signal. Another useful application is finding the purest control regions in an analysis, where one needs to maximize the presence of a certain process, or a kinematic characteristic.

A. Algorithm

Cut-points are read from a file of events that can consist of signal events, points randomly sampled about the signal, events from a signal-like model, events for a process for which a control region is to be defined; indeed, the cut-points can be based on any collection of events. The file from which cuts are read is referred to as the *cut file*. The signal and background

event files to which the cut-points are applied are referred to as *search files*. The type of cuts to be applied, which are described below, are specified in a *cuts definition file*. Conceptually, the core algorithm proceeds as follows. (The syntax [A] denotes a list of objects of type A.)

```

for cut-point in [cut-point]:
    for search-file in [search-file]:
        event-count = 0
        for (weight, point) in search-file:
            passed = true
            for cut in cut-point:
                if cut fails:
                    passed = false
                    break
            if passed:
                event-count = event-count + weight
write out event-counts for each cut-point

```

There is an obvious place to parallelize this algorithm using a PROOF-like system designed to run over multiple files in parallel, namely, the loop over search files. For example, rather than apply cut-points to a search file with 10^7 events, one could execute one hundred jobs in parallel each running over 10^5 events per search file. This requires no change to the existing RGS package. And, of course, one could split cut files across multiple jobs.

Associated with every (cut-point, search-file) pair is an **event-count** variable that accumulates the (weighted) sum of events that pass the cut-point. Therefore, every cut-point that is written out after the RGS algorithm has completed is associated with one or more event-count variables, one variable for each search-file. The event counts can be used to compute various statistical measures of signal significance in order to find the best cut-point, that is, the best set of cuts. The calculation of signal significances is a separate step performed on the output of the RGS algorithm.

A common measure of signal significance is (see, for example, the Statistics section in [35])

$$Z = \sqrt{2K(x)},$$

$$\text{where } K(x) = b[(1+x)\ln(1+x) - x], \quad \text{and } x = s/b, \quad (1)$$

which reduces to $Z = s/\sqrt{b}$ when $x \ll 1$, that is, when the signal is very much less than the background. Equation (1) can be derived from several perspectives. For example, if the data strongly favors the signal plus background distribution over the background-only distribution then it is likely that a signal is actually present. For discrete probability distributions, the Kullback-Leibler divergence [36]

$$D(P||Q) = \sum_n P(n) \ln \frac{P(n)}{Q(n)}, \quad (2)$$

is a parameterization-invariant measure of the dissimilarity between two distributions P and Q , which is zero if, and only if, $P = Q$. If we let $P(n) = \text{Poisson}(n, s+b)$, that is, the signal plus background probability distribution for count n , and we let $Q(n) = \text{Poisson}(n, b)$, the background-only probability distribution, it is readily shown that $D(P||Q) = K(x)$.

B. Cut types

In the original RGS implementation in the mid-1990s [27], only *one-sided* cuts were implemented:

$$\begin{aligned}
 x &> x_i, && \text{or,} \\
 x &< x_i, && \text{or,} \\
 |x| &> |x_i|, && \text{or,} \\
 |x| &< |x_i|, &&
 \end{aligned}
 \tag{3}$$

From these, higher dimensional cuts (cut-points) are constructed through the logical AND of one-sided cuts. For example, suppose we wish to select events based on the transverse momentum (p_T) and rapidity (y) of the highest p_T jet in each event. Each cut-point might be defined by

$$(p_T > p_{Ti}) \quad \& \quad (|y| < |y_i|), \tag{4}$$

that is, by the AND of the two one-sided cuts.

We have recently extended the RGS algorithm to permit the use of two other generic ways of imposing cuts: i) the *two-sided cuts*, e.g.,

$$(p_T > p_{Ti}) \quad \& \quad (p_T < p_{Tj}), \tag{5}$$

where the indices i and j denote different cut-points from the same cut file, and ii) the *staircase cuts*, which consist of the OR of cut-points for two or more variables, e.g.,

$$\begin{aligned}
 [(p_T > p_{Ti}) \quad \& \quad (|y| < |y_i|)] \quad \text{OR} \\
 [(p_T > p_{Tj}) \quad \& \quad (|y| < |y_j|)] \quad \text{OR} \\
 : & \quad :
 \end{aligned}
 \tag{6}$$

In order to create either a two-sided or a staircase cut, every cut-point in the cut file is associated with one or more randomly selected cut-points from the same file. One extra cut-point is needed to create a two-sided cut and typically several extra cut-points (defined by the number of steps in the staircase cut) are used to create a staircase cut. The current version of RGS therefore implements three classes of cut, that is, *cut types*, one-sided, two-sided, or staircase with the last two types formed from appropriate combinations of the cut types listed in Eq. (3). We provide detailed examples of the use of these cut types in Section III along with detailed syntax examples in the users manual in Appendix A.

III. PHYSICS EXAMPLES

As noted in the introduction, sophisticated multivariate methods of discrimination are now used routinely in particle physics. However, cut-based methods still have a useful role to play. One motivation is that the publication of cut-based benchmark analyses is an important service to the scientific community, especially to those who wish to reproduce published experimental results. The point is that, even if, for excellent reasons, one publishes an experimental result that uses a state-of-the-art multivariate discrimination method, it

is still of great value also to publish an optimized cut-based analysis that can be more readily reproduced by those not involved in the original analysis. On the experimental side, algorithms such as RGS provide a straightforward way to improve analyses by improving the cuts they use. Indeed, given the quantity of data at our disposal, there is really no good reason to dispense with cut optimization. Furthermore, optimized cut-based analyses provide benchmarks with respect to which the scientific utility of more sophisticated methods can be judged.

Since RGS is an algorithm for optimizing cuts, it can be applied to any set of variables. It may sometimes be advantageous to apply RGS to functions of these variables rather than to the original ones, such as the linear function that de-correlates them. In this case, the implied cuts on the original variables will, in general, no longer be orthogonal. Thus the RGS algorithm is more flexible than one might suppose despite its simplicity.

In this section, we show two examples of the use of RGS to produce optimized cut-based analyses. We first illustrate the one-sided and two-sided cut types using a simplified analysis of $H \rightarrow ZZ \rightarrow 4\ell$ final states. Then we show how all three RGS cut types can be employed in exploratory analyses that may suggest unexpected ways of selecting data.

A. Exploring $H \rightarrow ZZ \rightarrow 4\ell$ with RGS

The discovery of the Higgs boson at CERN in 2012 [5, 6] marked the completion of the Standard Model (SM) and brought to a close a fifty-year period of extraordinary advances in particle physics. Almost immediately, the Higgs boson went from a celebrated discovery to a prized tool in the search for new physics. One area in particular is receiving increasing attention, namely, the production of the Higgs boson in the vector boson fusion (VBF) mode (see, for example, Refs. [37–40]) in which weak vector bosons are radiated from initial state quarks and fuse to form a Higgs boson. New physics could modify details of weak vector boson fusion events.

We consider simplified analyses of the processes

$$p + p \rightarrow H \rightarrow Z/\gamma + Z/\gamma + X, \quad (7)$$

$$p + p \rightarrow Z/\gamma + Z/\gamma + X, \quad (8)$$

where the Z bosons decay to two charged leptons, either ee or $\mu\mu$, thereby producing final states with at least four charged leptons. The quantity X denotes additional objects in the final state. The dominant production mode of the Higgs boson is the gluon gluon fusion (ggF) process, while the dominant background arises from the production of two Z bosons without the intermediary Higgs boson, processes we shall refer to as the ZZ background. The principal experimental signature of vector boson fusion processes is the appearance of at least two high rapidity jets among the set of objects X . We consider one benchmark analysis, modeled on the CMS analysis of the 4-lepton final state [41] and three RGS optimized analyses.

Higgs boson VBF processes are challenging because their cross sections are smaller by an order of magnitude than those of the gluon gluon fusion (ggF) processes and they suffer from a paucity of distinctive features that distinguishes them from the ggF processes. Indeed, to date, only three moderately effective VBF/ggF discriminating observables have been identified; they are the number of jets—specifically, the requirement that there be at least two jets, the mass m_{jj} of the di-jet and $\Delta\eta_{jj}$, the absolute value of their rapidity difference.

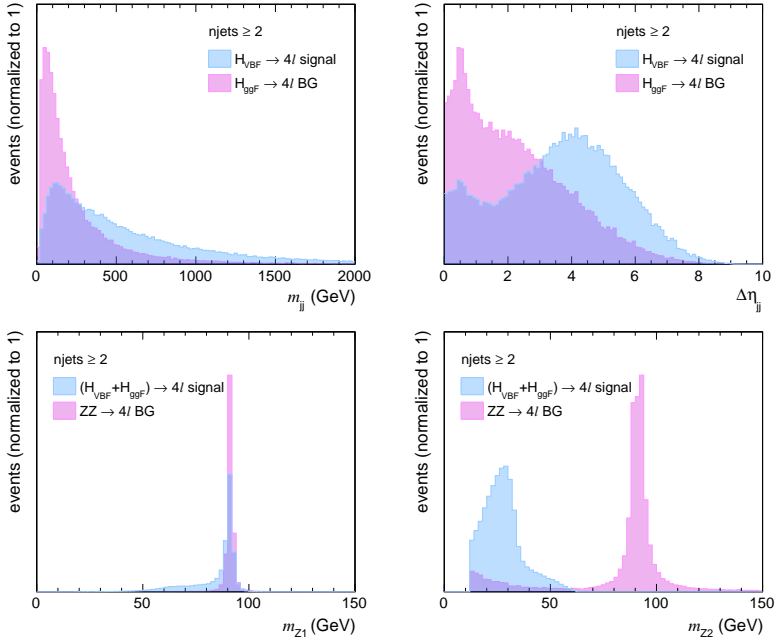


FIG. 2: (upper) Comparison of distributions of discriminating variables between the H_{VBF} signal and the H_{ggF} background processes (top row) and between Higgs boson events and the ZZ background (bottom row). (top left) the di-jet mass m_{jj} , (top right) the absolute value of the di-jet rapidity difference $\Delta\eta_{jj}$, (bottom left) the mass distribution of the di-lepton closest to the Z boson pole mass, which is referred to as Z_1 , and (bottom right) the same for the second di-lepton, which is referred to as Z_2 .

(Here, we neglect the jet masses and therefore do not distinguish between pseudo-rapidity, defined by $\eta = -2 \ln \tan \theta/2$ where θ is the polar angle, and the rapidity y .) The normalized distributions of the m_{jj} and $\Delta\eta_{jj}$ observables, together with the mass distributions of the Z bosons are shown in Figure 2. In our simplified analysis, we discriminate Higgs boson events from the ZZ background using the masses, m_{Z1} and m_{Z2} , of the two Z bosons, while the Higgs VBF and ggF processes are discriminated using the di-jet observables.

The three classes of proton-proton collision events, yielding four charged leptons in the final state, VBF Higgs (H_{VBF}), ggF Higgs (H_{ggF}), and ZZ , were generated at the LHC center of mass energy of 13 TeV using `PYTHIA8.209` [42, 43] with the Higgs boson mass set at 125 GeV. We approximate the response of the CMS detector with the public fast simulation package `Delphes v3.2.0` [44] tuned to reflect the latest published CMS electron and muon identification efficiencies [8, 45]. The default settings for `PYTHIA8` were used, together with a cut of > 10 GeV on the di-lepton masses (`PYTHIA8` parameter `23:mMin`). In addition, we impose a minimum transverse momentum (p_T) cut of 5 GeV (`PYTHIA8` parameter `PhaseSpace:pTHatMin`) on each of the products directly produced in the hard scatter. In particular, this is the minimum p_T of the Z bosons and of the forward quarks in the VBF processes. The cut is most relevant for the VBF processes and reduces the cross sections of the other processes by less than the quoted uncertainties in their predicted cross sections.

The ZZ cross section at next-to-leading (NLO) accuracy is computed using `POWHEG-BOX-V2/ZZ` [46], which for a minimum p_T cut on the di-lepton mass of 10 GeV

(POWHEG parameter `mllmin`) predicts a $p + p \rightarrow Z + Z \rightarrow e^+ + e^- + \mu + \mu^-$ cross section of 80.0 ± 1.1 fb and a $p + p \rightarrow Z + Z \rightarrow 4\ell$, $\ell = e, \mu$ cross section of 151.3 ± 2.4 fb. The calculations were done using the CT14nlo [47, 48] set of parton distribution functions (PDF) and cross-checked with MCFM v8.0 [49], which for the same di-lepton mass cut and PDF set gives a cross section of 89.7 ± 1.1 fb for the $ZZ \rightarrow e^+ + e^- + \mu + \mu^-$ process (MCFM process code `nproc 81`).

The cross sections for the VBF and ggF Higgs boson processes in the 4ℓ final states, with $\ell = e, \mu$, are taken from Ref. [50], which provides results computed at different levels of accuracy; we use the cross sections labeled as NNLO + NLL QCD + NLO EW. For the VBF processes, the cross section is 0.47 fb, computed as follows: $\sigma(qq \rightarrow H + qq) \times \text{BR}(H \rightarrow ZZ \rightarrow 4\ell)$, where $\sigma(qq \rightarrow H + qq) = 3.782$ pb and $\text{BR}(H \rightarrow ZZ \rightarrow 4\ell) = 1.25 \times 10^{-4}$, $\ell = e, \mu$. Similarly, the ggF cross section is taken to be $\sigma(gg \rightarrow H) \times \text{BR}(H \rightarrow ZZ \rightarrow 4\ell) = 5.52$ fb, where $\sigma(gg \rightarrow H) = 44.14$ pb. The calculations are for a Higgs boson of mass 125 GeV.

We simulated 3×10^5 , 10^6 , and 2×10^6 ggF, VBF, and ZZ events, respectively, and defined reconstructed leptons and jets with the following criteria.

- **Jets:** anti- k_T jets with a jet size $R = 0.4$, where $R = \sqrt{\Delta\eta^2 + \Delta\phi^2}$ and η and ϕ are the pseudo-rapidity and azimuthal angle, respectively. We required the jet $p_T > 20$ GeV, and jet $|\eta| < 4.7$.
- **Leptons (e and μ):** Generated leptons, to which the CMS lepton identification efficiencies are applied, with $p_T > 5$ GeV and $|\eta| < 2.4$ for muons and $p_T > 7$ GeV and $|\eta| < 2.5$ for electrons.

Events with at least two jets and four charged leptons are selected. The di-lepton with mass closest to the Z pole mass is labeled Z_1 , while the other di-lepton is labeled Z_2 . Both Z candidates are required to have a mass above 12 GeV. The relative efficiency of the event selection criteria in this simplified analysis was found to be 12.4%, 3.5%, and 1.8% for ggF, VBF, and ZZ, respectively.

Our benchmark analysis, with respect to which we can compare the results of the different RGS optimizations, imposes the additional cuts,

- leading lepton $p_T > 20$ GeV;
- next to leading lepton $p_T > 10$ GeV;
- $40 < m_{Z_1} < 120$ GeV, and
- $12 < m_{Z_2} < 120$ GeV,

which are the most important ones in the CMS Higgs to four-lepton analysis [41]. Furthermore, we required events to lie within the loose Higgs boson signal region defined by $100 < m_{4\ell} < 150$ GeV, where $m_{4\ell}$ is the 4-lepton mass. In this region, the Higgs boson signal is a narrow peak at 125 GeV, while the ZZ background is relatively flat. The results of the full selection (labeled CMS) are shown in Table I for an integrated luminosity of 100 fb^{-1} . This analysis of the three simulated event samples yields a Z significance of 1.03. Clearly, that number leaves considerable room for improvement, which is the goal of the RGS optimizations described next. In this paper, we use the significance measure defined in Equation (1).

TABLE I: Summary of the different Higgs optimizations (HOs) and results for the $H \rightarrow ZZ$ signals for and integrated luminosity of 100 fb^{-1} . All results are for events that lie in the Higgs boson signal region (see text), except for HO1, which uses events from the full phase space of the simulated events. Z_{max} is the maximum value of the Z significance. We use the significance measure defined in Eq. (1).

Opt	State	m_{jj}	$ \Delta\eta_{jj} $	m_{Z1}	m_{Z2}	N_S	N_B	Z_{max}
CMS	Analysis cuts (<i>var</i>)	–	–	40 – 120	12 – 120	H_{VBF} 5.78	$H_{\text{ggF}} + ZZ$ 29.48	1.03
HO1	Before opt. (<i>var</i>) (no $m_{4\ell}$ cut)	–	–	> 12	> 12	$H_{\text{VBF}+\text{ggF}}$	ZZ	
	Optimized vars	×	×	✓	✓			
	After opt. (<i>var</i>)	–	–	< 92.3	< 32.5	16.41	16.53	3.55
HO2	Before opt. (<i>var</i>)	–	–	> 12	> 12	$H_{\text{VBF}+\text{ggF}}$	ZZ	
	Optimized vars	×	×	✓	✓			
	After opt. (<i>var</i>)	–	–	58.4 – 94.6	17.0 – 52.1	20.06	5.80	6.10
HO3	Before opt. (<i>var</i>)	–	–	58.4 – 94.6	17.0 – 52.1	H_{VBF}	$H_{\text{ggF}} + ZZ$	
	Optimized vars	✓	✓	×	×			
	After opt. (<i>var</i>)	> 396.0	> 2.99	58.4 – 94.6	17.0 – 52.1	2.38	2.79	1.27

Three RGS optimizations are considered, each with 10^4 cut-points. Our strategy is to first find a subspace in which the event yield of Higgs boson events is enhanced relative to ZZ (in Higgs optimization HO2), and then, within that subspace, enhance the yield of VBF relative to ggF plus the remaining ZZ events (in HO3). The purpose of HO1 is merely to illustrate the use of the simplest form of cut, namely, one-sided cuts. These cuts are applied in the (m_{Z1}, m_{Z2}) plane in order to separate ggF+VBF events from ZZ events. Since Higgs boson events tend to populate the low m_{Z2} region, the appropriate one-sided cuts are $m_{Z1} < \text{cut}_1$ and $m_{Z2} < \text{cut}_2$, where the values of the tuple $(\text{cut}_1, \text{cut}_2)$ are determined by the distribution of ggF+VBF events in this plane. The results of the HO1 optimization, in which the $m_{4\ell}$ cut is omitted, are shown in Table I. The top left plot of Figure 3 shows the signal efficiency versus the background efficiency. The HO1 optimization yields a Z significance of 3.55.

The second optimization (HO2) searches for suitable two-sided cuts in the (m_{Z1}, m_{Z2}) plane. As is the case for HO1, the goal for HO2 is to discriminate between Higgs boson events and ZZ events, except that this time we require events to lie within the Higgs boson signal region, as defined above, and thereby benefit from the greatly reduced ZZ background within that region. The HO2 results are shown in Table I. The ggF+VBF signal efficiency versus the ZZ background efficiency is shown in the upper right plot of Figure 3 for different ranges of Z significance, while the best two-sided cuts of all those considered within the (m_{Z1}, m_{Z2}) plane is shown in the left plot of Figure 4. This pair of two-sided cuts yields a Z significance of 6.1.

It comes as no surprise that if one modifies HO1 by including in its definition the two-sided cut on $m_{4\ell}$ that defines the signal region, the Z significance improves; in fact, to

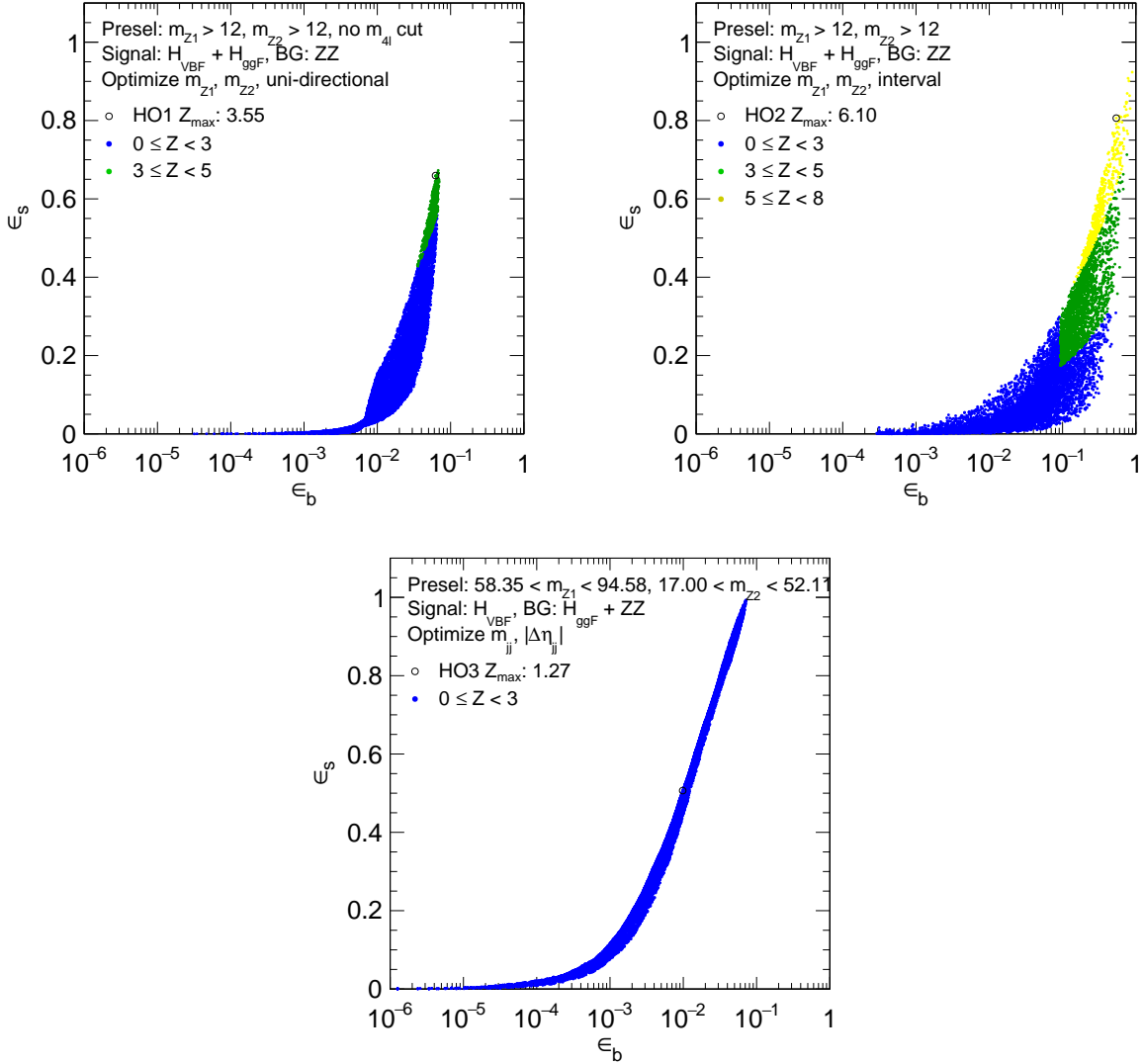


FIG. 3: Signal efficiency ϵ_s versus background efficiency ϵ_b , and Z significance ranges for the three different classes of optimization in this study: HO1 (top left), HO2 (top right), HO3 (bottom). For further details, see Table I.

4.84. What is notable is the fact that the optimal two-sided cuts in the (m_{Z1}, m_{Z2}) plane do considerably better. Indeed, for the modified HO1 optimization to achieve the same Z significance as HO2 would require the former to use 60% more data.

The third optimization (HO3) seeks to enhance VBF relative to ggF and ZZ by finding the optimal one-sided cuts, $m_{jj} > \text{cut}_1$ and $\Delta\eta_{jj} > \text{cut}_2$, for events constrained to lie within the two-sided cuts found by HO2. The results of HO3 are shown in Table I, while the lower plot of Figure 3 shows the signal efficiency versus the background efficiency and the right plot of Figure 4 shows the optimal one-sided cuts. The HO3 optimization yields a Z significance of 1.27, which is to be compared with 1.03 for our version of the CMS analysis. If analyses are restricted to cut-based methods, there is clearly more work to be done before an unambiguous VBF signal emerges in this channel. But, again, it is notable that 50%

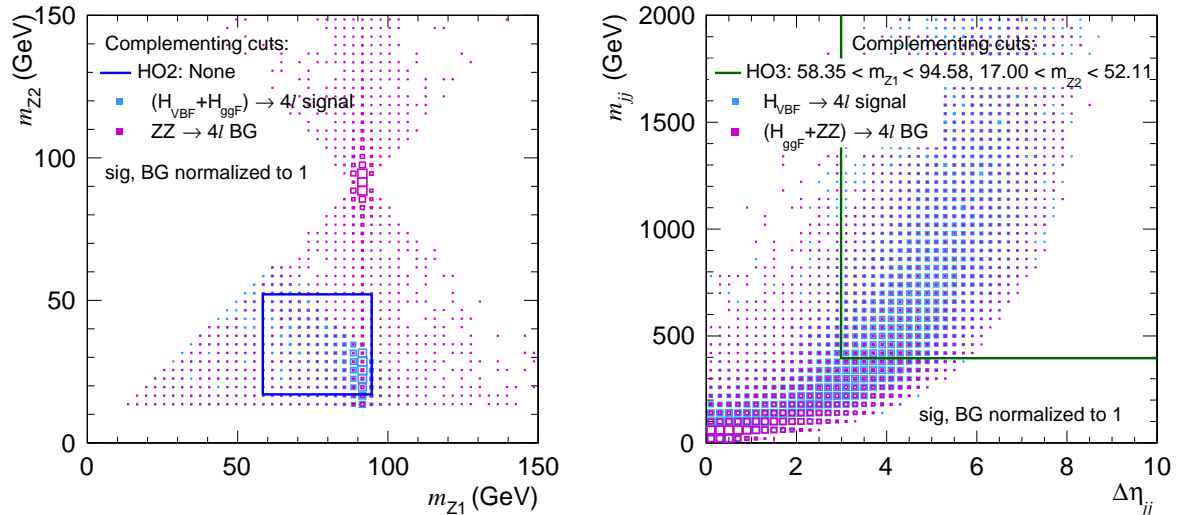


FIG. 4: The $m_{Z1} - m_{Z2}$ boundaries determined by the two-sided (i.e., box) cuts obtained using the HO2 optimization (left). The $|\Delta\eta|_{jj} - m_{jj}$ cut boundaries determined by the staircase cut using the HO3 optimization (right).

more data would be needed for the ‘‘CMS’’ analysis to match the results of HO3.

We chose this optimization problem because it is particularly challenging for a cut-based analysis due to the large overlap between the distributions for Higgs boson ggF and VBF events. It is already accepted that a precision measurement of the VBF cross section in the Higgs 4-lepton final state will require multivariate discriminants [41, 51] presumably constructed using machine learning methods. But, as noted in the introduction, cut-based analyses nevertheless remain useful as benchmarks that can be readily implemented. Moreover, the outputs of multivariate functions are merely sophisticated variables to which RGS can be applied if an optimal VBF region is needed.

In the next section, we describe a more sophisticated use of RGS optimization.

B. Optimizing SUSY razor boost with RGS

The random grid search is particularly useful for efficiently optimizing searches for new physics. We demonstrate its power and versatility by applying RGS to a supersymmetry (SUSY) search published by the CMS Collaboration [52]. This is a search for new physics in the jets, b jets and missing transverse energy (E_T^{miss}) final state that uses high momentum, that is, ‘‘boosted’’, W bosons whose decay products are merged into a single ‘‘fat’’ jet. The razor kinematic variables [34] are used to discriminate possible SUSY signals from the Standard Model (SM) backgrounds. The analysis mainly targets gluino decays to top squark-top quark pairs.

To illustrate how RGS can be useful in designing searches, we selected a SUSY signal point with parameters that lead to a gluino with mass of 1355 GeV, a light top squark with mass of 409 GeV and a lightest neutralino with mass of 252 GeV. The remaining sparticles are heavy and inaccessible at the 13 TeV LHC. In this scenario, gluinos decay exclusively

to $\tilde{t}_1 t$ pairs, where the momenta of the top quarks are high due to the large $m(\tilde{g}) - m(\tilde{t}_1)$ mass difference. Subsequently, since the mass difference $m(\tilde{t}_1) - m(\tilde{\chi}_1^0)$ is smaller than $m(t)$, top squarks directly decay to $Wb\tilde{\chi}_1^0$. This decay structure leads to multiple jets, multiple b jets, and a significant fraction of events with boosted W bosons coming from the top quarks produced directly in the gluino decays. The dominant SM background for this signal is $t\bar{t}$ +jets. For simplicity, we consider only this background process in this study. For the signal point, we calculated the SUSY mass spectrum from the given SUSY parameter point using the `SOFTSUSY v3.3.1` package [53], and the sparticle decays using the `SUSYHIT` package [54] (with `SDECAY 1.5` and `HDECAY 3.4`). For both the signal and background, we used `PYTHIA8.209` [42, 43] to generate LHC events at 13 TeV. As was done for the Higgs boson study, the response of the CMS detector was simulated using `Delphes v3.2.0` [44]. We calculated the NLO cross section for the SUSY signal using the `Prospino 2` package [55, 56], and obtained 21.2 fb. For $t\bar{t}$ +jets, we used the NLO+NLL value calculated by the ATLAS and CMS Collaborations centrally using the `Top++v2.0` package, which is 815.96 fb for a top quark mass of 173.2 GeV [57–61]. Simulated events were weighted to correspond to 30 fb^{-1} of integrated luminosity. The output `ROOT` event files were analyzed using `TNManalyzer` [62].

We then implemented the following object definitions.

- **Jets:** anti- k_T jets with jet size $R = 0.4$. Jet $p_T > 30$ GeV, $|\eta| < 2.4$.
- **b jets:** Jets defined as above, that pass the default `Delphes` b jet tagger.
- **W jets:** Cambridge-Aachen jets with jet size $R = 0.8$. Jet mass of $60 < m_j < 120$ GeV, n-subjettiness value [63] $\tau_2/\tau_1 < 0.5$.
- **Leptons (e and μ):** Lepton isolation $\sum_{\Delta R} p_T/p_T^\ell < 0.1$, where $\Delta R < 0.5$, and lepton $p_T > 5$ GeV, $|\eta| < 2.5$.
- **Missing transverse energy:** negative vector sum of transverse momenta of all visible objects.

Based on these object definitions, events were selected that have at least 2 jets and no leptons. For these events, we calculated the razor kinematic variables M_R and R^2 as described in [34]. For the RGS optimizations, we use the discriminating variable set consisting of the number of jets (n_j), number of b jets (n_b), number of W jets (n_W), leading jet p_T (p_T^{j1}), M_R and R^2 . Figure 5 compares the distributions of these six variables for the SUSY signal and $t\bar{t}$ +jets background, and confirms that each variable has indeed some measure of discrimination between the signal and the background.

The original CMS study selects events with $n_j \geq 3$, $n_b \geq 1$, $n_W \geq 1$ and $p_T^{j1} > 200$ GeV (the “preselection”), followed by the simple razor selection $M_R > 800$ GeV and $R^2 > 0.08$, which gives 140.1 signal events, 10702.4 background events, and a corresponding Z value of 1.35. In the following, we optimize selections based on the above discriminant (cut) variables in order to improve the signal significance, quantified by the Z value defined in Equation (1). A summary of these optimization studies and their results is given in Table II.

In the first SUSY optimization, SO1, we simply implement the CMS preselection and attempt to improve the razor selection through optimizing M_R and R^2 using a 2-dimensional, 20 step, staircase cut. The top left frame of Figure 6 shows the signal efficiencies ϵ_s versus background efficiencies ϵ_b and Z significance intervals obtained for each candidate staircase

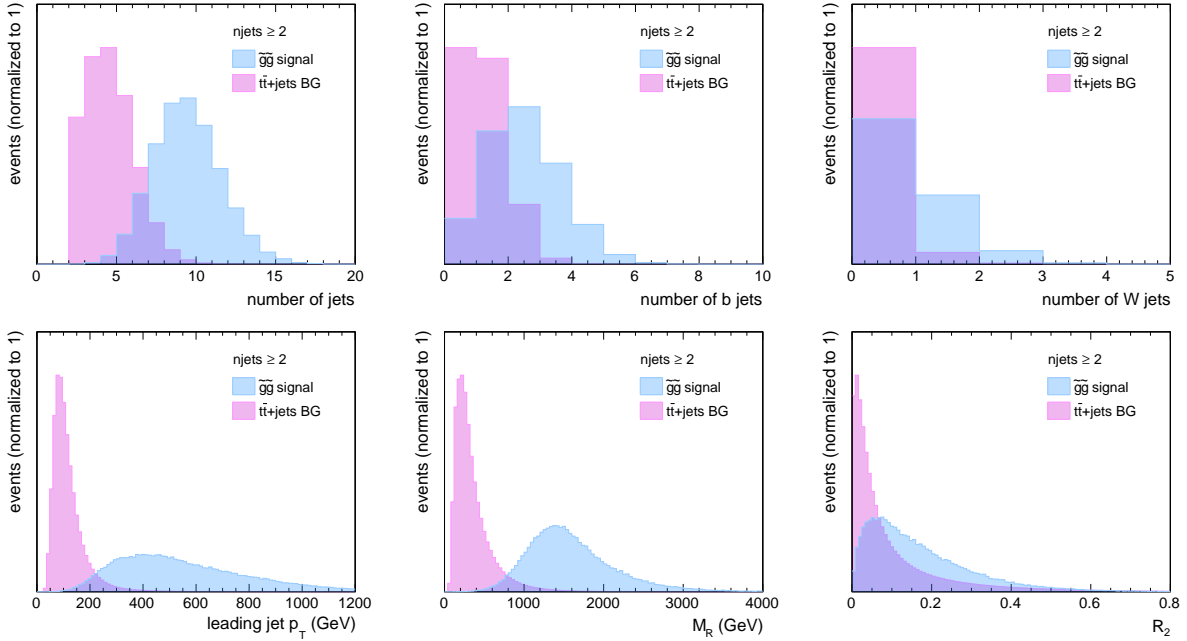


FIG. 5: Comparison of distributions for discriminating variables between the $\tilde{g}\tilde{g}$ signal and the $t\bar{t}$ -jets background.

cut. As for the Higgs studies, the cut with the largest Z significance is taken to be the optimal selection. The optimal M_R - R^2 selection in this case has a Z value of 3.7, resulting from signal and background counts of $N_S = 85$ and $N_B = 504$ respectively. The associated cut is shown in the right frame of Figure 7 as the red curve.

Next, in optimization SO2a, we again implement the preselection, but this time optimize over all six variables, with one-sided cuts on n_j , n_b , n_W , p_T^{j1} , and a 2-dimensional, 20 step staircase cut on M_R - R^2 . For this case, ϵ_s versus ϵ_b distributions and Z intervals are given in the top left frame of Figure 6, which shows that including all variables in the optimization can dramatically improve the selection performance. The optimal selection with the best Z value of 9.07 is given in Table II and the left frame of Figure 7. This selection includes a cut of $n_j \geq 9$, which restricts us to a high multiplicity phase space, where a fully reliable event reconstruction becomes harder to achieve. Furthermore, this selection results in low event yields, which would lead to large uncertainties. In order to overcome these issues, we look for a cut set where the cut value for n_j , denoted by n_j^{cut} , is at most 6. The optimal selection in this case, SO2b, has $n_j \geq 6$, a Z value of 4.72, and is shown in Table II and the left frame of Figure 7.

The above study with the requirement of at least one boosted W boson already demonstrates the power of the RGS algorithm in finding diverse options in improving event selections. The RGS algorithm can also be used for easy exploration of alternative signatures for a given signal. To illustrate this, we start with a much simpler preselection of $n_j \geq 3$, and optimize over all six cut variables. Figure 6 (lower frame) shows that the more open phase space makes it possible to reach much lower ϵ_b for a given ϵ_s , and consequently higher Z significances. The optimal selection for the most generic optimization, denoted as SO3a, is given in Table II and Figure 7, and has a very high Z significance of 13.25. This optimization

TABLE II: Summary of the different SUSY optimizations (SOs) and results for the $\tilde{g}\tilde{g}$ signal over the $t\bar{t}$ +jets background for an integrated luminosity of 30 fb^{-1} . Z_{max} is the maximum value of the Z significance. We use the significance measure defined in Eq. (1).

Opt	State	n_j	n_b	n_W	p_T^{j1}	M_R, R^2	N_S	N_B	Z_{max}
CMS	Analysis cuts (<i>var</i>)	≥ 3	≥ 1	≥ 1	> 200	$M_R > 800$ $R^2 > 0.08$	140.1	10702.4	1.35
SO1	Before opt. (<i>var</i>)	≥ 3	≥ 1	≥ 1	> 200	–			
	Optimized vars	×	×	×	×	✓			
	After opt. (<i>var</i>)	≥ 3	≥ 1	≥ 1	> 200	Fig 7, left	85.2	504.2	3.69
SO2a	Before opt. (<i>var</i>)	≥ 3	≥ 1	≥ 1	> 200	–			
	Optimized vars	✓	✓	✓	✓	✓			
	After opt. (<i>var</i>)	≥ 9	≥ 3	≥ 1	> 285.6	Fig 7, left	31.3	4.9	9.07
SO2b	Before opt. (<i>var</i>)	≥ 3	≥ 1	≥ 1	> 200	–			
	Optimized vars	✓	✓	✓	✓	✓			
	Cut value req. (var^{cut})	3-6	–	–	–	–			
	After opt. (<i>var</i>)	≥ 6	≥ 2	≥ 1	> 293.7	Fig 7, left	73.6	220.3	4.72
SO3a	Before opt. (<i>var</i>)	≥ 3	–	–	–	–			
	Optimized vars	✓	✓	✓	✓	✓			
	After opt. (<i>var</i>)	≥ 11	≥ 2	≥ 0	> 263	Fig 7, right	59.4	7.3	13.25
SO3b	Before opt. (<i>var</i>)	≥ 3	–	–	–	–			
	Optimized vars	✓	✓	✓	✓	✓			
	Cut value req. (var^{cut})	3-6	–	–	–	–			
	After opt. (<i>var</i>)	≥ 6	≥ 3	≥ 0	> 312	Fig 7, right	107.1	161.6	7.68

is achieved when the requirement $n_W \geq 1$ is lifted, but it has a very high jet multiplicity requirement of $n_j \geq 11$, which brings with it the same issues as in the SO2a optimization. To avoid these issues, we again choose the best cut set for which $n_j^{cut} \leq 6$, SO3b, and which has a Z significance of 7.68 and cut values shown in Table II and Figure 7 right frame.

The RGS optimization can be very helpful in finding complementary approaches when searching for a given signal. Here, we have shown that the $\tilde{g}\tilde{g} \rightarrow t\bar{t}t\bar{t}_1 \rightarrow t\bar{t}\tilde{\chi}_1^0 t\bar{t}\tilde{\chi}_1^0$ signal can be explored with the razor kinematic variables in final states with boosted W bosons, or in generic hadronic final states with b jets. Overall, RGS showed that final states with high jet multiplicities (detector conditions permitting) are the most sensitive to new physics, independently of whether or not one requires the presence of boosted W bosons. Comparing the left and right frames of Figure 7 shows that selections with boosted W bosons favor higher M_R values. RGS can be easily used for learning the characteristics of the cut phase space. For example, the four frames in Figure 8 show the 2-dimensional histograms of the number of cut sets for Z significance versus n_j^{cut} , $p_T^{j1, cut}$, n_b^{cut} and n_W^{cut} respectively for SO3. These histograms show that the highest Z values can be obtained for $n_j^{cut} \sim 10$, $p_T^{j1, cut} \sim 200-300$, $n_b^{cut} \sim 2-3$, and $n_W^{cut} = 0$. Similarly, Figure 9 shows the average Z significance value on the z -axis versus cut values of different cut variables on the x - and y axes, which

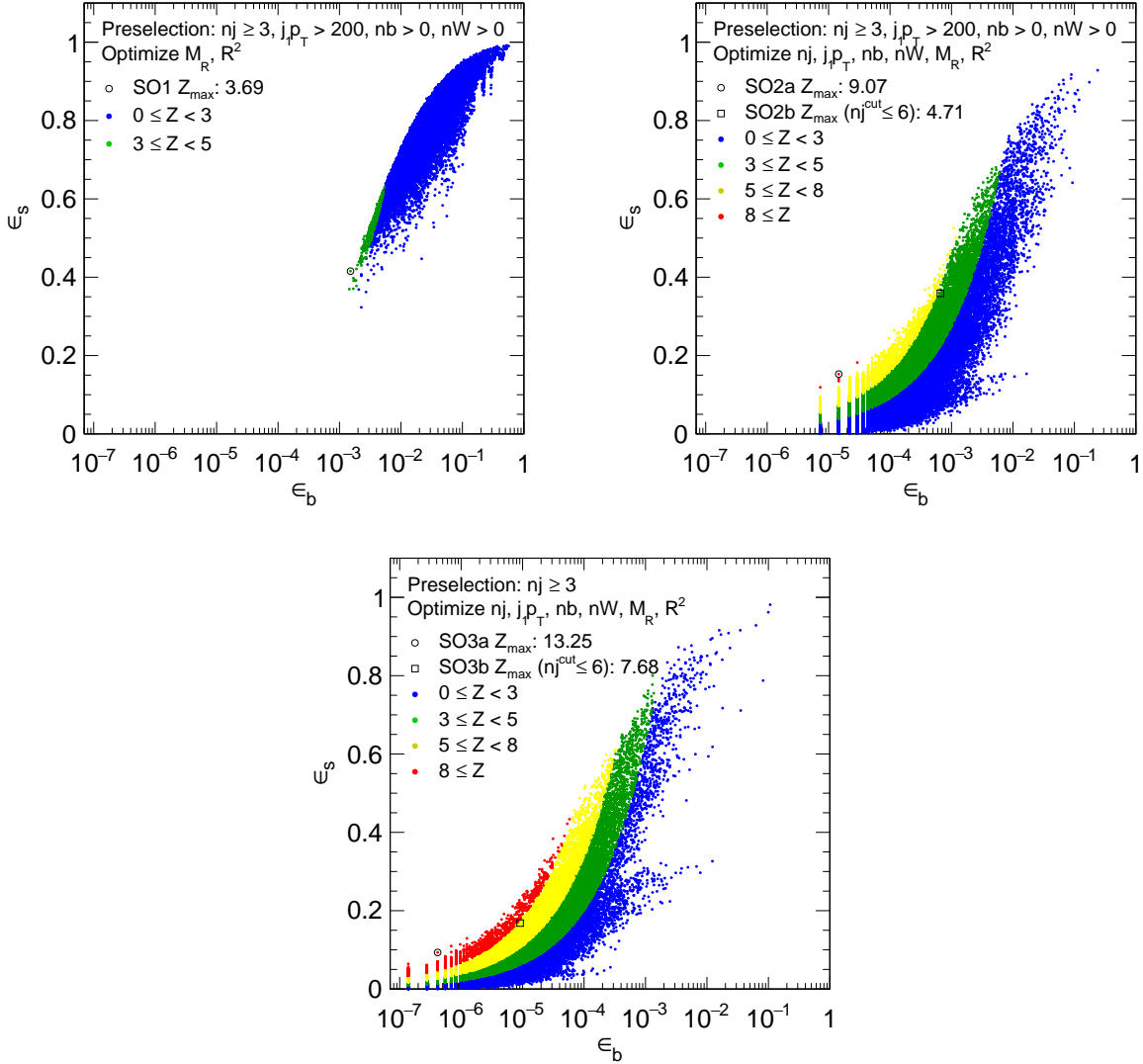


FIG. 6: Signal efficiency ϵ_s versus background efficiency ϵ_b , and Z significance ranges for the three different classes of optimizations in this study: SO1 (top left), SO2a and SO2b (top right), SO3a and SO3b (bottom). See further details in Table II.

could help to characterize the best cut value combinations for different variables.

IV. SUMMARY

We have described a simple algorithm called the random grid search that efficiently optimizes event selections by randomly searching for cuts in the region of the cuts phase space where the cuts are likely to be most useful. Furthermore, we have described recent enhancements to RGS, specifically, the addition of two-sided cuts, and a cut type we call a staircase cut that is the OR of two or more sets of one-sided cuts on two or more variables. Next, we presented two examples which showed the effectiveness of RGS optimization in

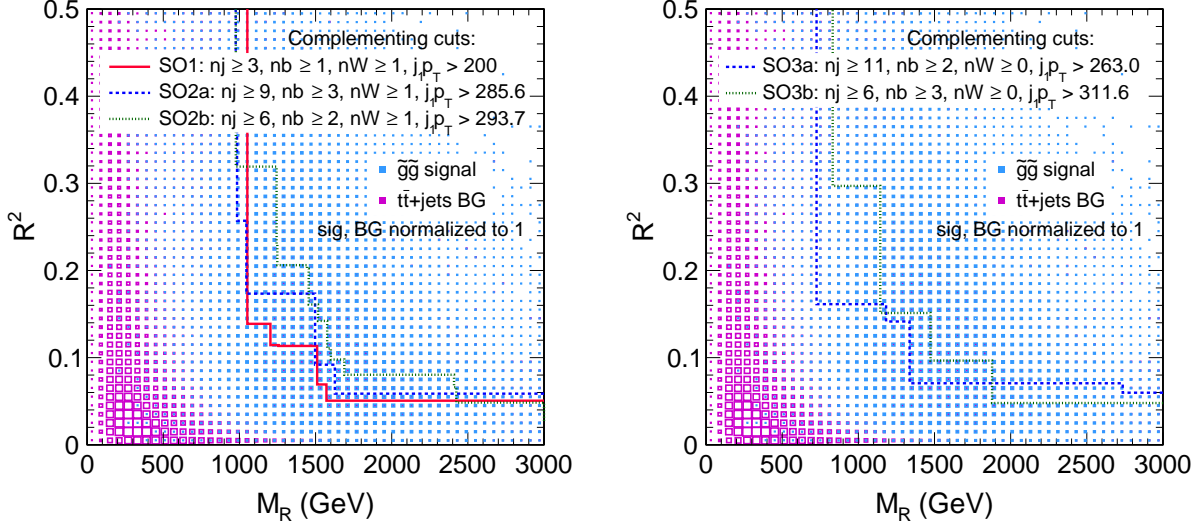


FIG. 7: M_R - R^2 cut boundaries determined by 20 step 2-dimensional staircase cuts in the 5 different optimizations in this study. Cut boundaries are shown for optimizations with a preselection requiring (left) and not requiring (right) a boosted W boson. Both frames also show the M_R - R^2 distributions for the $\tilde{g}\tilde{g}$ signal and the $t\bar{t}$ +jets background.

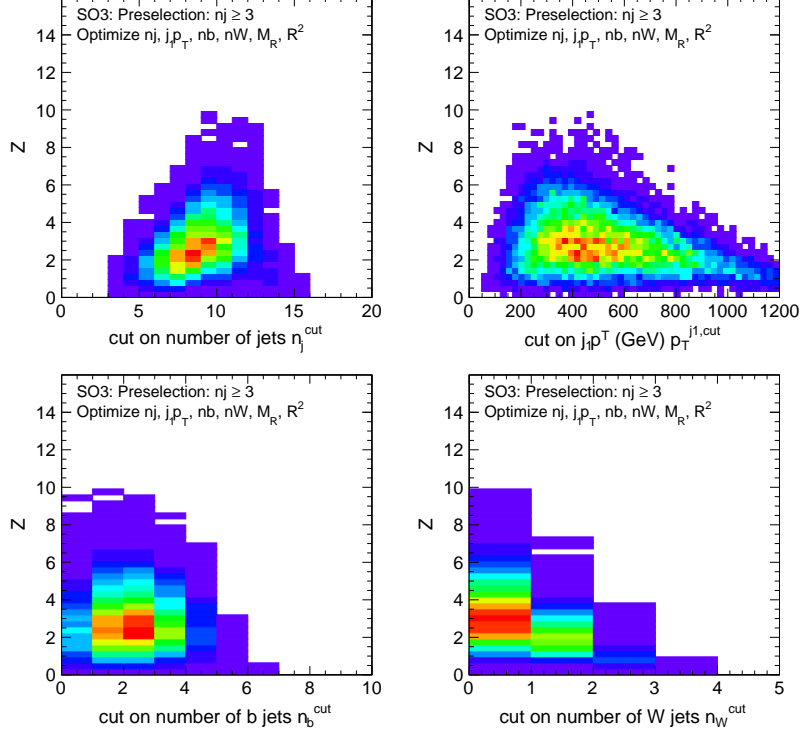


FIG. 8: 2-dimensional histograms of number of cut sets for Z significance versus n_j^{cut} (top left), $p_T^{j1,cut}$ (top right), n_b^{cut} (bottom left) and n_W^{cut} (bottom right) for the SO3-type optimization.

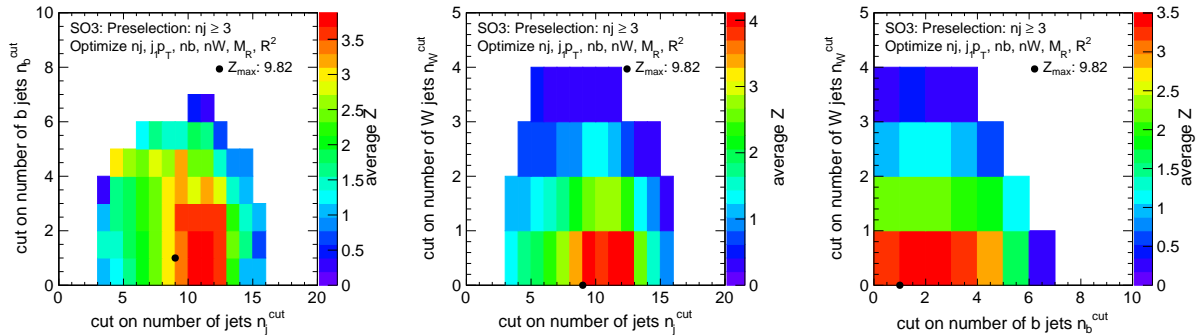


FIG. 9: The average value on the z -axis versus cut values of different cut variables on x - and y axes.

exploring the impact of different cuts on different sets of variables.

It is undoubtedly true that for the most difficult analyses, in which optimality is at a premium, multivariate discriminants constructed using machine learning will likely win the day over any cut-based analysis. However, that expectation does not obviate the utility of optimal cut-based analyses. A significant fraction of LHC analyses are still cut-based. Feasibility studies of almost all searches are done using cut-based analyses. Furthermore, there are circumstances in which a region enhanced in some way is needed, perhaps a control region for an analysis, which is to be determined by cuts applied to one or more variables. These variables could themselves be sophisticated multivariate discriminants. Then, a simple, effective, way to find the optimal cuts, such as the random grid search, would be useful. There are, of course, other algorithms to search for optimal cuts. One that has found some favor in particle physics finds cuts using a genetic algorithm. However, we would argue that sophistication of this kind is unnecessary for most cut-based analyses and an algorithm like RGS is perfectly adequate. Moreover, it is easy to envisage further useful developments. Indeed, one obvious development would be to extend the staircase cut to permit the use of two-sided cuts that will make it possible to find the OR of quite general multi-dimensional bounded regions. Work towards this is in progress.

Acknowledgements

The work of PCB and HBP is supported in part by the U.S. Department of Energy, under contract number DE-AC02-07CH11359 with Fermilab, and under grant number de-sc0010102, respectively. The work of SS is supported by the financial support of the National Research Foundation of Korea (NRF), funded by the Ministry of Science & ICT under contract NRF-2008-00460 and by the U.S. Department of Energy through the Distinguished Researcher Program from the Fermilab LHC Physics Center.

Appendix A: Using RGS

The RGS algorithm comprises two independent steps. The first imposes a set of event selections based on selection variables and cut directions defined by the user, and corresponding cut values taken from a set of specified events (usually signal events), and it determines

the resulting signal and background efficiencies and counts for each selection. These efficiencies and counts are then used in the second step to compute a measure of signal significance, which can be maximized over different selections in order to determine the optimal event selection.

The efficiency of the algorithm derives from the fact that the search for cuts is stochastic and determined by (in most applications) the predicted signal distribution. In effect, this distribution provides an importance sampled set of cuts. Consequently, the algorithm is less subject to the “curse of dimensionality” and the accuracy of the results, as is true of Monte Carlo integration, is independent of the dimensionality of the cut space. The accuracy rather depends on the sample sizes. The examples released with the package run in minutes. But, since the time to run is roughly proportional to the product of the number of cuts and the number of events to which the cuts are applied, for large sample sizes the RGS algorithm can take several hours. However, RGS can be trivially parallelized simply by splitting the events to which cuts are to be applied into many batches, running RGS in parallel, and, for each cut, summing the signals and backgrounds from each batch.

Running the RGS package requires C++, Python and ROOT with PyROOT built in. The package can be obtained from `github` and compiled as follows.

```
git clone https://github.com/hbprosper/RGS.git
cd RGS
source setup.(c)sh
make
```

The package is released with code for the two examples described in this paper, in the directory tree

```
RGS/examples
    /data
    /Higgs
        /H01
        /H02
        /H03
    /SUSY
        /S01
        /S02
        /S03
```

The ROOT files used in the Higgs and SUSY examples should be downloaded and unpacked into the `data` directory using, for example, the commands

```
wget http://www.hep.fsu.edu/~harry/RGS/data/SUSY.tar.gz
tar zxvf SUSY.tar.gz
```

The package contains a single C++ class called `RGS` that is callable from Python. Instructions for running the examples are provided in the `README` file in the `examples` directory. For each example, the event variables and cut directions to be used for optimization are specified in a text file with a simple syntax. The signal and background events can be input in simple text format or as ROOT trees. Using ROOT trees has the significant advantage that it is possible to apply selection criteria to the events that are to be used in the search for cuts.

Below we give a more detailed description of the variables and cut directions file and the RGS class.

1. Variables and cut directions file

The variables and cut directions to be used in the optimization are input to RGS through a text file with a specific syntax. The variable names should correspond to the variable names in the cut and search datafiles. Currently RGS allows optimization with three types of cuts, which could be input as follows:

- **One-sided cuts:** These are simple cuts like $p_T > x$, $|\eta| \leq y$, etc. The syntax is:

```
variable-name  cut-direction
```

The available types are:

- `var <` : $var < value$
- `var >` : $var > value$
- `var <=` : $var \leq value$
- `var >=` : $var \geq value$
- `var <|` : $|var| < value$
- `var >|` : $|var| > value$
- `var ==` : $|var| = value$

- **Two-sided cuts:** These are cuts with two boundaries, as in the case of $x < m_{\ell\ell} < y$. The two boundaries are taken from two separate events in the signal event list. The syntax is

```
variable-name  cut-direction
```

The two-sided cut type syntax is:

- `var <>` : $value1 < var < value2$

- **Staircase cuts:** (initially inspired by the razor kinematic variables M_R and R^2): In 2-dimensional space, this cut can be visualized as a sideview of a non-uniform staircase. The staircase cut is constructed by selecting N events from the signal, and for each event (or cutset i), taking the AND of a set of M one-sided cuts. The selection becomes the OR of the phase space covered by the N cutsets. The syntax is as follows:

```
\staircase number-of-steps N (i.e., cut-points)
  variable-name-a cut-direction-a
  variable-name-b cut-direction-b
  ...
  variable-name-M cut-direction-M
\end
```

and a concrete example can be written as

```

\staircase N
    var_a >
    var_b >
    ...
    var_M <
\end

```

which would give

$(var_a > value_a^1 \text{ and } var_b > value_b^1 \dots \text{ and } var_M < value_M^1)$ or
 $(var_a > value_a^2 \text{ and } var_b > value_b^2 \dots \text{ and } var_M < value_M^2)$ or
...
 $(var_a > value_a^N \text{ and } var_b > value_b^N \dots \text{ and } var_M < value_M^N)$.

The staircase cut construction can accommodate cut types $<$, $>$, $<=$, $>=$, $< |$ and $| >$.

Below are some example variable and cut direction inputs used in this study:

```

# Simple one-sided cuts
njet >=
j1pT >

# Two-sided cut
Z2mass <>

# Staircase cut
\staircase 4
    MR >
    R2 >
\end

```

The cut definition files used in the Higgs and SUSY examples in this paper are named

examples/Higgs/H0i.cut, $i = 1, 2, 3$

and

examples/SUSY/S0i.cut, $i = 1, 2, 3$

2. The RGS class

The RGS class is found in `src/RGS.cc` and `include/RGS.h`. The functionalities and methods of the class are as follows.

- Constructors:

```

RGS(std::string (or std::vector<std::string>&) cutdatafilename,
    int start=0,
    int numrows=0,

```

```
std::string treename="",
std::string weightname="",
std::string selection="");
```

where

- `cutdatafilenames` are the names of one or more files containing the cut values, usually files with signal events. The files can be in ROOT or text format as described above. In a Python program, multiple file names can be specified in a vector of strings using the PyROOT wrapper `vector('string')`.
 - `start` is the row or event where we start reading the cut values.
 - `numrows` is the number of rows to be selected from the cuts file; `-1` specifies that all rows are to be read. The number of rows read will in general be greater than the number of selected rows if a selection has been applied when using a ROOT n-tuple.
 - `treename` is the name of the ROOT tree to be read. Tree names should be the same for the signal and background events used in RGS. If omitted, the file to be read is presumed to be a text file.
 - `weightname` is an optional variable that gives the name of the ROOT branch or text column that contains the event weight.
 - `selection` is an optional selection string to be used for selecting rows. This is a ROOT feature and so can only be used with ROOT files.
- Add a search file, or a list of searchfiles, which contain the signal and background event data:

```
void add(std::string (or std::vector<std::string>&) searchfilename,
        int start=0,
        int numrows=-1,
        std::string resultname="",
        double weight=1.0);
```

where

- `searchfilename` are the names of one or more files with signal and background data. Again, multiple files can be specified in Python programs using the PyROOT `vector` wrapper. All files should be in the same format.
 - `start`, `numrows` as described above.
 - `resultname` is appended to the count and fraction variables. e.g. , “_s” for signal, “_b” for background. If omitted, the ordinal value of the search file, starting at zero, is appended to the count and fraction variables.
 - `weight` is an optional (multiplicative) event weight assigned per search file.
- Run the RGS algorithm for specified cut variables and cut directions: This can be done either using a cut definition file, which was described above:

```
void run(std::string varfile, // file name of Variables file
        int nprint=500);
```

or by directly specifying cuts as strings:

```
void run(vstring& cutvar, // Variables defining cuts
        vstring& cutdir, // Cut direction (cut-type)
        int nprint=500);
```

- Return results:

- Return the total (possibly weighted) count for the data file identified by `dataindex`:

```
double total(int dataindex);
```

- Return the (possibly weighted) count for the given data file and the given cut-point:

```
double count(int dataindex, int cutindex);
```

- Return all variables read from the cut file(s):

```
vstring& vars();
```

- Return number of cuts:

```
int ncuts();
```

- Return cut values for cut-point identified by `cutindex`.

```
vdouble cuts(int cutindex);
```

- Return cut variable names

```
vstring cutvars();
```

- Return number of events for a specified data file.

```
int ndata(int dataindex);
```

- Return values for data given data file and event.

```
vdouble& data(int dataindex, int event);
```

- Save resulting counts and fractions to a text or a ROOT file with name `filename` (if `.root` is found in file name, a ROOT file is saved, otherwise, a text file is saved):

```
void save(std::string filename);
```

3. Running RGS

The examples released with the RGS package show how to use the RGS class and how to analyze its results. The examples use Python, but the RGS class can be used in either a C++ or Python program.

Each example can be run by executing the command

```
./train.py
```

which instantiates an `RGS` object and calls the relevant methods to add signal and background files, run the `RGS` algorithm, and write the results to a `ROOT` file. (Note that due to the length of the SUSY signal and background datasets, the SO3 optimization could take more than an hour. Here is a clear case in which splitting the search files into multiple files and running `RGS` in parallel would speed things up considerably. SO1 and SO2 each take about 10 minutes.) The results in the `ROOT` file can be analyzed by running

```
./analysis.py
```

which calculates the Z value defined in Eq. (1) for each cut and finds the best cut (the one with the largest Z value). A ROC curve of signal and background efficiencies is also plotted. A collection of helpful utility functions may be found in `python/rgsutil.py`, which can be imported using

```
from rgsutil import *
```

For example, the utility class `OuterHull` draws the outer hull of a staircase cut from given set of 2-dimensional cut values.

-
- [1] P. C. Bhat, *Ann. Rev. Nucl. Part. Sci.* **61**, 281 (2011).
 - [2] C. M. Bishop, *Pattern Recognition and Machine Learning* (Springer, 2006), ISBN ISBN 978-0-387-31073-2, URL <http://www.springer.com/us/book/9780387310732>.
 - [3] B. Abbott et al. (D0), *Phys. Rev.* **D58**, 052001 (1998), hep-ex/9801025.
 - [4] V. M. Abazov et al. (D0), *Phys. Rev. Lett.* **103**, 092001 (2009), 0903.0850.
 - [5] S. Chatrchyan et al. (CMS), *Phys. Lett.* **B716**, 30 (2012), 1207.7235.
 - [6] G. Aad et al. (ATLAS), *Phys. Lett.* **B716**, 1 (2012), 1207.7214.
 - [7] G. Aad et al. (ATLAS), *JINST* **11**, P04008 (2016), 1512.01094.
 - [8] V. Khachatryan et al. (CMS), *JINST* **10**, P06005 (2015), 1502.02701.
 - [9] A. M. Sirunyan et al. (CMS) (2017), 1712.07158.
 - [10] R. Aaij et al. (LHCb), *JINST* **10**, P06013 (2015), 1504.07670.
 - [11] P. Baldi, P. Sadowski, and D. Whiteson, *Nature Commun.* **5**, 4308 (2014), 1402.4735.
 - [12] P. Baldi, P. Sadowski, and D. Whiteson, *Phys. Rev. Lett.* **114**, 111801 (2015), 1410.3469.
 - [13] P. Baldi, K. Bauer, C. Eng, P. Sadowski, and D. Whiteson, *Phys. Rev.* **D93**, 094034 (2016), 1603.09349.
 - [14] D. Guest, J. Collado, P. Baldi, S.-C. Hsu, G. Urban, and D. Whiteson, *Phys. Rev.* **D94**, 112002 (2016), 1607.08633.
 - [15] J. Searcy, L. Huang, M.-A. Pleier, and J. Zhu, *Phys. Rev.* **D93**, 094033 (2016), 1510.01691.
 - [16] A. Aurisano, A. Radovic, D. Rocco, A. Himmel, M. D. Messier, E. Niner, G. Pawloski, F. Psihas, A. Sousa, and P. Vahle, *JINST* **11**, P09001 (2016), 1604.01444.
 - [17] R. Acciarri et al. (MicroBooNE), *JINST* **12**, P03011 (2017), 1611.05531.
 - [18] A. Hoecker, P. Speckmayer, J. Stelzer, J. Therhaag, E. von Toerne, and H. Voss, *PoS ACAT*, 040 (2007), physics/0703039.
 - [19] M. Feindt and U. Kerzel, *Nucl. Instrum. Meth.* **A559**, 190 (2006).
 - [20] F. Pedregosa, G. Varoquaux, A. Gramfort, V. Michel, B. Thirion, O. Grisel, M. Blondel, P. Prettenhofer, R. Weiss, V. Dubourg, et al., *Journal of Machine Learning Research* **12**, 2825 (2011).

- [21] F. Chollet et al., *Keras*, <https://github.com/keras-team/keras> (2015).
- [22] M. Abadi, A. Agarwal, P. Barham, E. Brevdo, Z. Chen, C. Citro, G. S. Corrado, A. Davis, J. Dean, M. Devin, et al., *TensorFlow: Large-scale machine learning on heterogeneous systems* (2015), software available from tensorflow.org, URL <https://www.tensorflow.org/>.
- [23] M. Abadi, P. Barham, J. Chen, Z. Chen, A. Davis, J. Dean, M. Devin, S. Ghemawat, G. Irving, M. Isard, et al., in *12th USENIX Symposium on Operating Systems Design and Implementation (OSDI 16)* (2016), pp. 265–283, URL <https://www.usenix.org/system/files/conference/osdi16/osdi16-abadi.pdf>.
- [24] Theano Development Team, arXiv e-prints [abs/1605.02688](https://arxiv.org/abs/1605.02688) (2016), URL <http://arxiv.org/abs/1605.02688>.
- [25] M. Ballintijn, M. Biskup, R. Brun, G. Ganis, G. Kicking, A. Peters, F. Rademakers, P. Canal, and D. Feichtinger, *Nucl. Instrum. Meth.* **A559**, 13 (2006).
- [26] P. C. Bhat, H. B. Prosper, and C. Stewart (1993-1994), unpublished.
- [27] N. A. Amos, C. Stewart, P. Bhat, C. Cretsing, E. Won, W. G. D. Dharmaratna, and H. B. Prosper, in *Proceedings, 8th International Conference on Computing in High-Energy and Nuclear Physics (CHEP 1995): Rio de Janeiro, Brazil, September 18-22, 1995* (1995), pp. 215–219.
- [28] S. Abachi et al. (D0), *Phys. Rev. Lett.* **74**, 2632 (1995), hep-ex/9503003.
- [29] F. Abe et al. (CDF), *Phys. Rev. Lett.* **74**, 2626 (1995), hep-ex/9503002.
- [30] V. M. Abazov et al. (D0), *Phys. Rev.* **D64**, 092004 (2001), hep-ex/0105072.
- [31] V. M. Abazov et al. (D0), *Phys. Rev.* **D67**, 012004 (2003), hep-ex/0205019.
- [32] S. Chatrchyan et al. (CMS), *JHEP* **04**, 033 (2012), 1203.3976.
- [33] N. C. Strobbe, Master’s thesis, Gent U. (2011), URL <http://inspirehep.net/record/1088189/files/openfile.pdf>.
- [34] C. Rogan (2010), 1006.2727.
- [35] C. Patrignani et al. (Particle Data Group), *Chin. Phys.* **C40**, 100001 (2016).
- [36] S. Kullback and R. A. Leibler, *Ann. Math. Statist.* **22** (1), 79 (1951).
- [37] C. Collaboration (CMS) (2016).
- [38] T. A. collaboration (ATLAS) (2016).
- [39] M. Aaboud et al. (ATLAS), *JHEP* **11**, 112 (2016), 1606.02181.
- [40] M. Cacciari, F. A. Dreyer, A. Karlberg, G. P. Salam, and G. Zanderighi, *Phys. Rev. Lett.* **115**, 082002 (2015), 1506.02660.
- [41] S. Chatrchyan et al. (CMS), *Phys. Rev.* **D89**, 092007 (2014), 1312.5353.
- [42] T. Sjostrand, S. Mrenna, and P. Z. Skands, *JHEP* **05**, 026 (2006), hep-ph/0603175.
- [43] T. Sjostrand, S. Mrenna, and P. Z. Skands, *Comput. Phys. Commun.* **178**, 852 (2008), 0710.3820.
- [44] J. de Favereau, C. Delaere, P. Demin, A. Giammanco, V. Lematre, A. Mertens, and M. Selvaggi (DELPHES 3), *JHEP* **02**, 057 (2014), 1307.6346.
- [45] S. Chatrchyan et al. (CMS), *JINST* **8**, P11002 (2013), 1306.6905.
- [46] P. Nason and G. Zanderighi, *Eur. Phys. J.* **C74**, 2702 (2014), 1311.1365.
- [47] S. Dulat, T.-J. Hou, J. Gao, M. Guzzi, J. Huston, P. Nadolsky, J. Pumplin, C. Schmidt, D. Stump, and C. P. Yuan, *Phys. Rev.* **D93**, 033006 (2016), 1506.07443.
- [48] A. Buckley, J. Ferrando, S. Lloyd, K. Nordstrm, B. Page, M. Rfenacht, M. Schnherr, and G. Watt, *Eur. Phys. J.* **C75**, 132 (2015), 1412.7420.
- [49] J. M. Campbell, R. K. Ellis, and W. T. Giele, *Eur. Phys. J.* **C75**, 246 (2015), 1503.06182.
- [50] D. de Florian et al. (LHC Higgs Cross Section Working Group) (2016), 1610.07922.

- [51] G. Aad et al. (ATLAS), *Phys. Rev.* **D91**, 012006 (2015), 1408.5191.
- [52] V. Khachatryan et al. (CMS), *Phys. Rev.* **D93**, 092009 (2016), 1602.02917.
- [53] B. C. Allanach, *Comput. Phys. Commun.* **143**, 305 (2002), hep-ph/0104145.
- [54] A. Djouadi, M. M. Muhlleitner, and M. Spira, *Acta Phys. Polon.* **B38**, 635 (2007), hep-ph/0609292.
- [55] W. Beenakker, R. Hopker, and M. Spira (1996), hep-ph/9611232.
- [56] W. Beenakker, R. Hopker, M. Spira, and P. M. Zerwas, *Nucl. Phys.* **B492**, 51 (1997), hep-ph/9610490.
- [57] M. Czakon and A. Mitov, *Comput. Phys. Commun.* **185**, 2930 (2014), 1112.5675.
- [58] M. Czakon, P. Fiedler, and A. Mitov, *Phys. Rev. Lett.* **110**, 252004 (2013), 1303.6254.
- [59] M. Czakon and A. Mitov, *JHEP* **01**, 080 (2013), 1210.6832.
- [60] M. Czakon and A. Mitov, *JHEP* **12**, 054 (2012), 1207.0236.
- [61] P. Brnreuther, M. Czakon, and A. Mitov, *Phys. Rev. Lett.* **109**, 132001 (2012), 1204.5201.
- [62] Prosper, H. B. and Sekmen, S., CMS Internal Note CMS-IN-2012-012, CERN (2012), URL <http://cdsweb.cern.ch/record/1279362>.
- [63] J. Thaler and K. Van Tilburg, *JHEP* **03**, 015 (2011), 1011.2268.